

Photodegradation of phenol in aqueous solution using Mn/TiO₂ catalysts

H. Abdelouahab-Reddam¹, Z. Abdelouahab-Reddam¹, R. El Mail¹, and A. Aaliti²

¹Equipe de Recherche Chimie de l'Eau et Pollution Atmosphérique, Département de Chimie,
Faculté des Sciences, Université Abdelmalek Essaâdi,
Avenue de Sebta, Mhannech II, B.P. 93002, Tétouan, Maroc

²Département de génie chimique,
Faculté des Sciences et Techniques, Université Abdelmalek Essaâdi,
Ancienne Route de l'Aéroport, Km 10, Ziaten, B.P. 416, Tanger, Maroc

Copyright © 2014 ISSR Journals. This is an open access article distributed under the **Creative Commons Attribution License**, which permits unrestricted use, distribution, and reproduction in any medium, provided the original work is properly cited.

ABSTRACT: Mn/TiO₂ catalysts were prepared and evaluated for the photocatalytic degradation of phenol. Two different methods of preparation had been investigated: Sol-gel and impregnation processes. The prepared samples were characterized by TGA-TDA, adsorption of N₂ at -196 °C, XRD, Raman and FTIR. Products analysis was carried out by gas chromatography (GC). The total capacity obtained for phenol photodegradation, on the prepared catalysts, was rather promising. Indeed, we practically obtained a total degradation of phenol (97.3%) for a contact time of 10 min.

KEYWORDS: photocatalysis; water, titania; sol-gel; impregnation; phenol; oxidation; degradation.

1 INTRODUCTION

Recently, widespread water contamination by phenol has been postulated as a topic of an ever-increasing importance. Phenol is a well-known potential carcinogen agent for human being and is of a considerable health concern, even at low concentration. Hence, the treatment of wastewater containing phenol is a challenging task. Many technologies have been investigated for the removal and the degradation of phenolic compounds in wastewater such as adsorption, biodegradation, extraction by liquid membrane, oxidation, etc. The oxidation has shown their potential to decompose phenol completely in wastewater. In this context, the aim of the present study is to develop TiO₂-based catalysts for the degradation of phenol by means of photocatalysis.

Titania (TiO₂) is widely used for the removal of highly toxic and non-biodegradable pollutants frequently presents in wastewater by means of photocatalysis. This oxide can be used pure or doped by other metals or metallic oxides. In most cases, doped TiO₂ exhibits a higher photoactivity than the pure one. Brezová et al. [1] reported that the presence of some metals such as Li⁺, Zn²⁺ and Pt⁰ enhances the photoactivity of titania in the degradation of phenol and that the photoactivity of these materials depends strongly on the character and the concentration of the employed dopant.

In this sense, this paper focuses on the photocatalytic activity of pure and modified titania in the removal of phenol in aqueous solution. Concretely, the aim of the present study is to prepare manganese-based catalysts supported on TiO₂, following two different methods: sol-gel and impregnation, in order to investigate the influence of the preparation method on their physico-chemical properties and their activity in photocatalytic oxidation of phenol.

2 MATERIALS AND METHOD

2.1 TiO₂ PREPARATION

TiO₂-SG was prepared by the sol-gel method, from titanium (IV) isopropoxyde Ti(C₁₂H₂₈O₄) (97%, Aldrich). The further was used as a titanium and oxygen precursor owing to its molecular structure, which represents the originality of the present study. Titania was prepared according to the following molar ratios: Ti(C₁₂H₂₈O₄): 6 C₂H₅OH: 16 H₂O. Thus, an amount of Ti(C₁₂H₂₈O₄) was added dropwise to a solution of water and ethanol while stirring continuously, at constant temperature (70 °C), during 4 h until the gel formation. After the gelation was completed, the gels were dried at 70 °C for 24 h and calcined at 400, 500 and 600 °C for 12 h, using a heating rate of 10 °C.min⁻¹. It is worth noting that the pH was controlled at 3.

2.2 Mn/TiO₂ CATALYSTS PREPARATION

As mentioned above, two different Mn/TiO₂ catalysts preparation methods (sol-gel and impregnation) were used in order to evaluate the effect of the preparation method on the chemical and textural properties of the elaborated catalysts.

Mn/TiO₂(SG) samples prepared by sol gel process were obtained by the same procedure as for the pure titania. Thus, an aqueous solution of Mn(NO₃)₂.4H₂O containing the appropriate amount to obtain a Mn loading of 5 wt.% was added to the Ti(C₁₂H₂₈O₄) in H₂O/HNO₃ solution. Obtained samples were calcined at 400 and 600 °C for 12 h (10 °C.min⁻¹), as described previously.

In the case of the Mn/TiO₂ (Imp) catalysts prepared by the impregnation method, two supports have been used: TiO₂-SG previously prepared by sol-gel and a commercial Degussa P25 titania (TiO₂-P25) (86.43 % anatase and 13.66 % rutile). The supports have been impregnated with an aqueous solution of Mn(NO₃)₂.4H₂O. The suspension was heated at 80 °C and kept under stirring during 4 h. Then, the samples were dried during 24 h at 110 °C and calcined at 550 °C for 6 h (10 °C.min⁻¹). As in the case of Mn/TiO₂-SG samples, the Mn content was of 5 wt.%.

2.3 CHARACTERIZATION OF CATALYSTS

Thermogravimetric analysis was carried out using an SDT-Q600 analyzer, TA Instruments. Concretely, this study was carried out under an oxidant atmosphere (synthetic air flow of 100 ml.min⁻¹), over the temperature range from 25 to 1000 °C using a heating rate of 10 °C.min⁻¹. Weight loss was recorded as a function of temperature.

The N₂ adsorption isotherms were carried out, at -196 °C, using a fully automated Micromeritics 3-Flex Surface Characterization Analyzer. The specific surface area (*S*_{BET}) was obtained by applying the B.E.T method to the experimental N₂ adsorption data.

The X-ray diffraction patterns of the catalysts were recorded on a X'Pert Pro MPD diffractometer from Panalytical, fitted with a Cu anode. The average crystal size for TiO₂ was estimated by application of the Scherrer equation:

$$d = \frac{K\lambda}{\beta \cos \theta_B}$$

Where K is the constant whose value is approximately 0.9, λ is the wavelength of the X-ray radiation source (0.154 nm), β is the full width at half maximum intensity (FWHM) (rad), and θ_B is the Bragg angle at the position of the peak maximum.

The content of anatase was also calculated applying the Spurr-Myers equation:

$$A\% = \frac{100}{1 + 1.265 \left(\frac{I_R}{I_A} \right)}$$

Where I_R is the intensity of the rutile (110) peak, and I_A is the intensity of the anatase peak (101) signal.

Raman measurements were obtained by using a FRA 106/S FT-Raman spectrometer, covering a spectral range of 70-3500 cm⁻¹ for stokes and 100-2000 cm⁻¹ for anti-stokes. This equipment has a near infrared excitation laser source (Nd-YAG) and a high sensitivity liquid N₂-cooled Ge.

IR analysis presented in the present study was carried out using a FT-IR spectrometer (model VERTEX 70), which covers a very wide spectral range, from 100 to 7000 cm⁻¹ with a resolution of 0.5 cm⁻¹.

2.4 LIQUID-PHASE DEGRADATION OF PHENOL

The photoactivity of the samples has been evaluated in the photocatalytic degradation of phenols in aqueous solution under UV irradiation. A phenol aqueous solution was prepared by dissolving an amount of phenol in water in order to obtain a final concentration of 10^{-3} mol/L. An aqueous suspension of 100 ml of phenol solution containing 100 mg of catalyst was stirred during 1 h in the dark to achieve the adsorption-desorption equilibrium, and then, irradiated in a closed box with a UV light, which emitted the UV radiation with wavelength of 254 nm. The evolution of reaction was followed taking samples of the suspension (1 ml) in different time intervals (5, 10, 20, 30, 40, 50 and 60 min). In order to remove photocatalyst particles before analyses, the mixtures were filtered using microfilters with a pore size opening of 20 μm . Phenol concentrations in the different sample were determined by means of chromatography, using a VARIAN CP-3380 chromatograph, and a CP-Wax 52 CB column with 30 m length, 0.25 mm internal diameter and 0.25 μm film thickness.

3 RESULTS AND DISCUSSION

3.1 CHARACTERIZATION

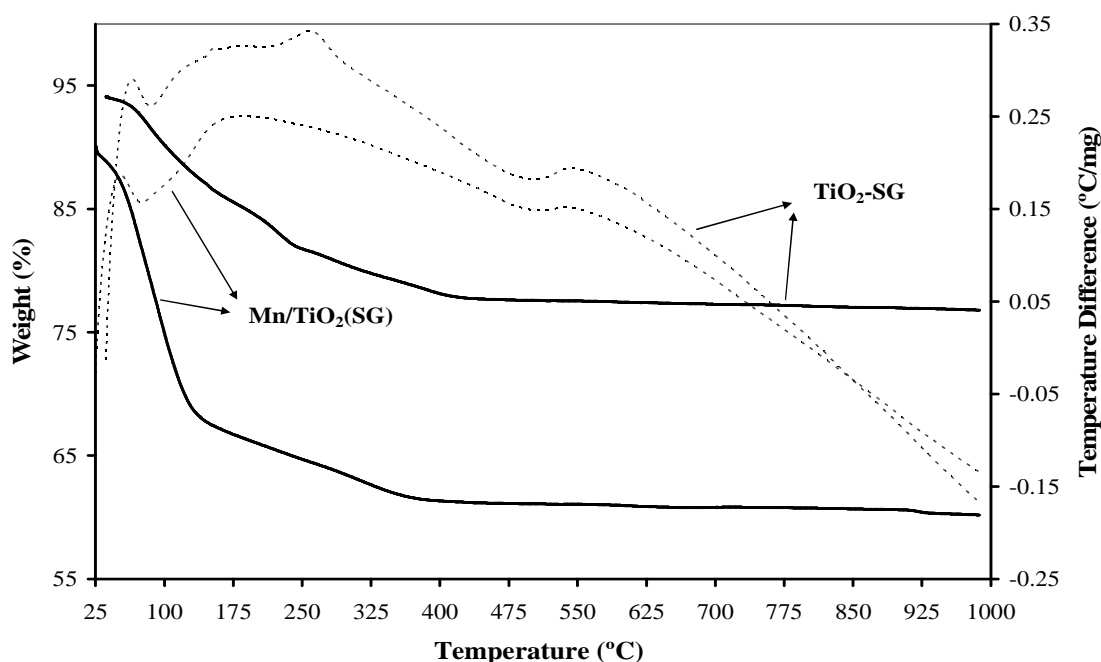


Fig. 1. TG-DTA curves for TiO₂-SG and Mn/TiO₂(SG) samples.

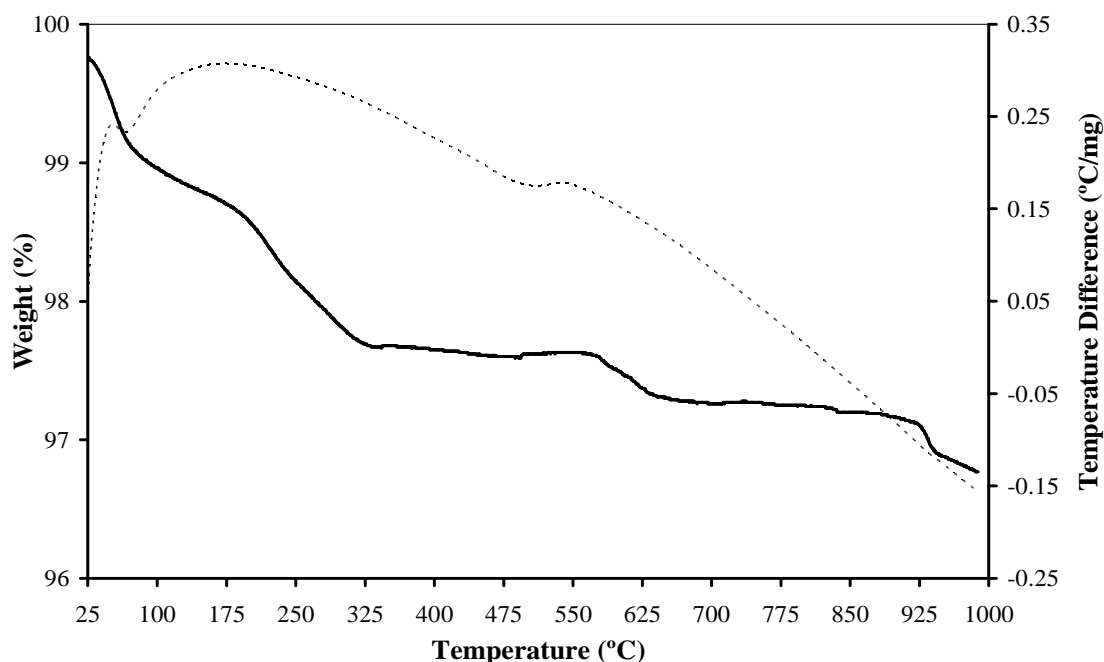


Fig. 2. TG-DTA curves for Mn/TiO₂-P₂₅ (Imp) sample.

Fig. 1 shows the TG-DTA profiles of TiO₂-SG and Mn/TiO₂(SG) prepared by sol-gel. Both samples show two different processes of weight loss with different rates. The first stage from, approximately, 100 °C to 250 °C, with an endothermic peak in the DTA curve, can be associated to the evaporation of adsorbed water. The second stage of weight loss at about 250-400 °C, corresponding to a broad exothermic peak, could be attributed to the residual organic compounds decomposition (solvents and precursors) as well as the crystallization of amorphous state into anatase. The exothermic peak which appears around 600 °C could be related to the anatase-rutile transformation. It is interesting to note that the final weight loss of Mn/TiO₂(SG) sample is more important compared with TiO₂(SG), which could be due to the decomposition of nitrates from the manganese precursor in Mn/TiO₂(SG) sample. Fig. 2 shows the TG-DTA profile of Mn/TiO₂-P₂₅(Imp) prepared by impregnation method. The sample exhibit a profile similar to that obtained for the sol-gel prepared samples. However, the weight loss is considerably lower with respect to these samples.

Table 1: Specific surface B.E.T for the different prepared samples

Sample	$S_{BET}(\text{m}^2 \cdot \text{g}^{-1})$	$V_{micro}(\text{cm}^3 \cdot \text{g}^{-1})$	$V_{meso}(\text{cm}^3 \cdot \text{g}^{-1})$
TiO ₂ - SG (400 °C)	127	0.05	0.20
TiO ₂ - SG (600 °C)	24	0.01	0.04
TiO ₂ -P25	53	0.02	0.34
Mn/TiO ₂ -P25 (SG-400 °C)	134	0.05	0.16
Mn/TiO ₂ -P25 (SG-600 °C)	87	0.03	0.12
Mn/TiO ₂ -SG (Imp-550 °C)	7	0.00	0.03
Mn/TiO ₂ -P25 (Imp-550 °C)	45	0.02	0.12

Table 1 resumes the results of textural characterization of the studied samples. These results were deduced from the data of N₂ adsorption at -196 °C and subatmospheric pressure. In the case of TiO₂ prepared using sol-gel process, the BET surface area decrease considerably with increasing the calcination temperature. This can be explained by an increase of the particle size during the calcination, which leads to a reduction of the interparticle distance in the structure. The introduction of manganese produces a decrease of the BET surface of this material, due to a partial blockage of the porosity by manganese particles. However, the introduction of manganese on the commercial titania (Mn/TiO₂-P25 (Imp-550 °C)) result in a augmentation of BET surface area. Shalan et al. [2] also observed an increase in the surface area value after the incorporation of manganese. This author relates this rise with the introduction of manganese into the interstitial sites of TiO₂ lattice leading

to a decrease in the crystallite size. On the other hand, the surface area of this material (Mn- modified titania) decrease with increasing the calcination temperature. This result suggests that a proportion of manganese was not incorporated into the support and some Mn particles are dispersed on the TiO₂ surface. Thus, the increase of the calcination temperature produces a sintering of these particles as has been mentioned above.

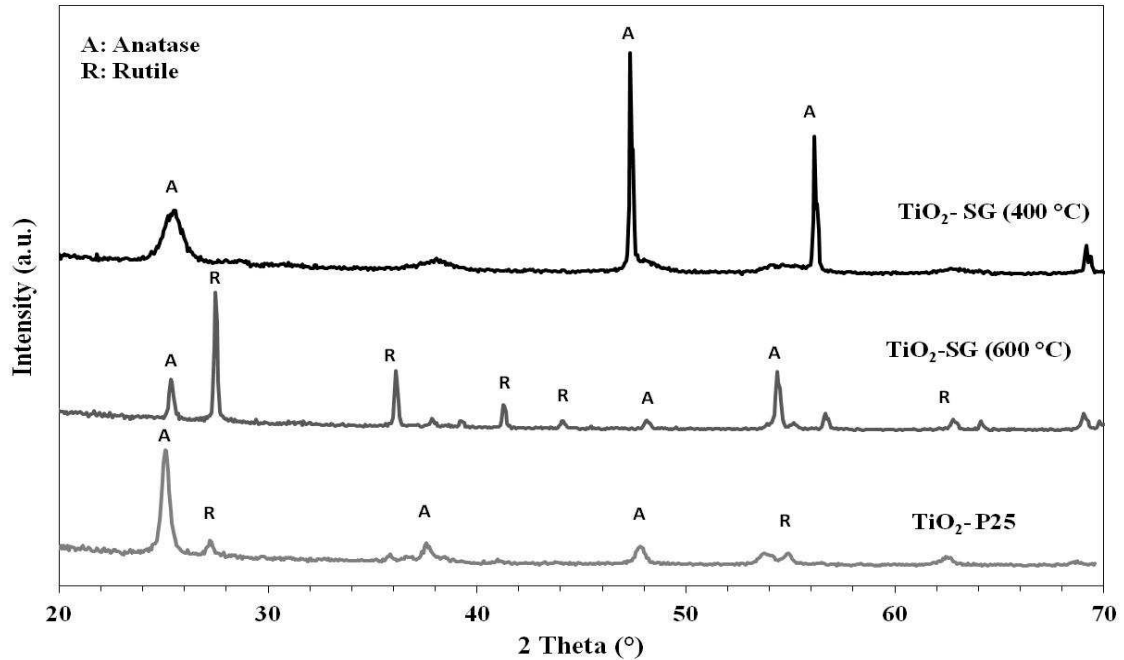


Fig. 3. XRD patterns of the commercial TiO₂-P25 and TiO₂-SG calcined at 400 and 600 °C.

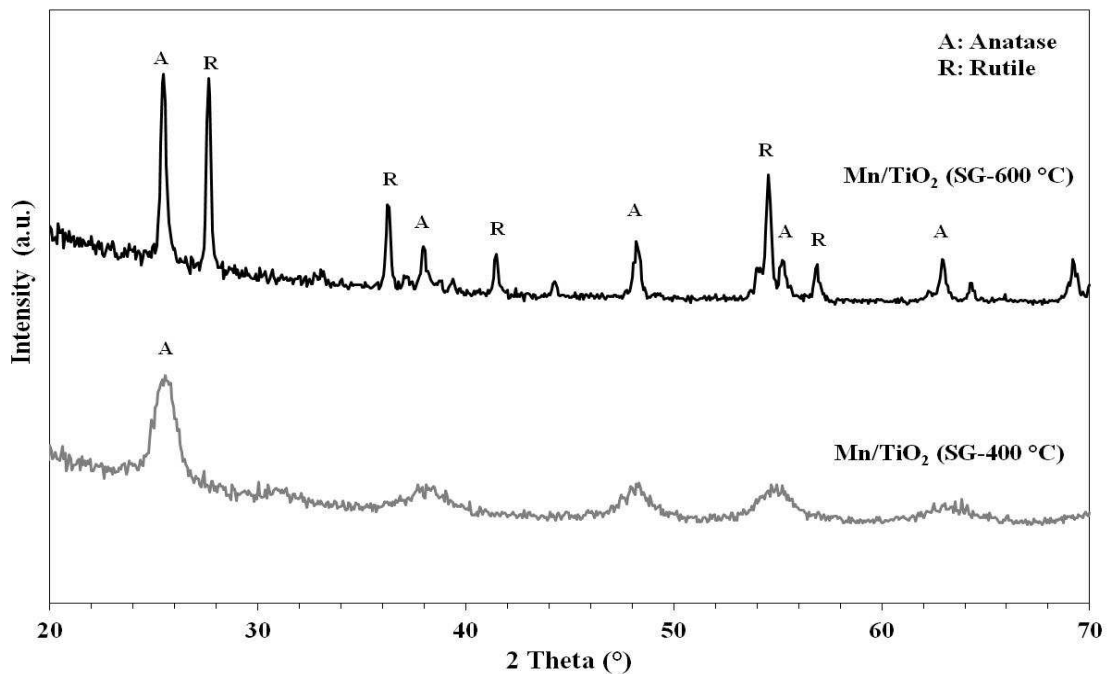


Fig. 4. XRD patterns of Mn/TiO₂ samples prepared by sol-gel and calcined at 400 and 600 °C.

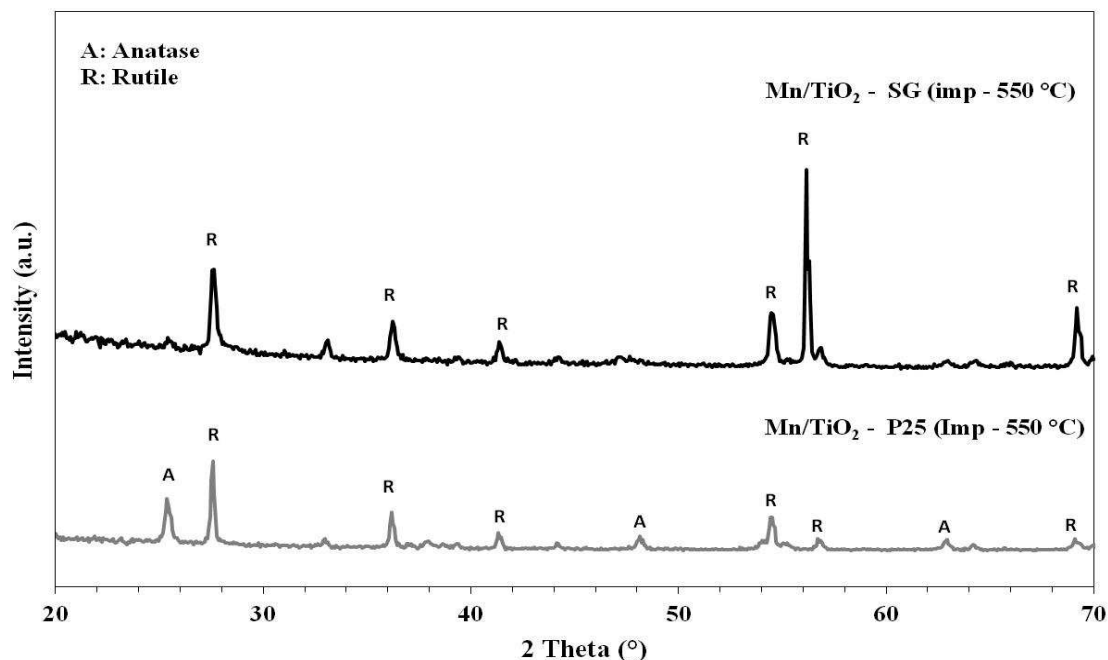


Fig. 5. XRD patterns of Mn/TiO₂-P25 and Mn/TiO₂-SG prepared by impregnation and calcined at 550 °C.

Table 2: Properties of the samples obtained from XRD analysis.

Simple	Phase	2 θ (°)	Cristallite size (nm)	% A	%R
TiO ₂ - SG (400 °C)	A	25.42	10.29	100	0
TiO ₂ - SG (600 °C)	A	25.37	30.89	20.54	79.46
	R	27.49	41.35		
TiO ₂ -P25	A	25.49	24.71	86.34	13.66
	R	27.62	20.67		
Mn/TiO ₂ (SG-400 °C)	A	25.54	7.17	100	0
Mn/TiO ₂ (SG-600 °C)	A	25.39	30.89	43.86	56.14
	R	27.56	41.35		
Mn/TiO ₂ -SG (Imp-550 °C)	R	27.59	31.01	0	100
Mn/TiO ₂ -P25 (Imp-550 °C)	A	25.39	30.87	27.92	72.08
	R	27.56	31.01		

Fig. 3 shows XRD patterns of the commercial TiO₂-P25 and TiO₂-SG calcined at 400 and 600 °C. Additionally, the data obtained from X-ray diffractograms of some samples are summarized in Table. 2. It can be seen that the increase of the calcination temperature produces the transformation of a proportion of anatase to rutile. Indeed, in the sample calcined at 400 °C all the peaks can be attributed to the anatase phase, while the diffractogram of the same sample calcined at 600 °C exhibits some peaks related to rutile phase. Furthermore, XRD patterns indicate that the calcination temperature has a significant effect on the crystalline size of TiO₂. Thus, the peaks of the same phase of anatase are broader in the case of the sample calcined at lower temperatures, which may be related to a sintering of the particles after treatment at high temperatures. The XRD diffractograms of Mn/TiO₂ (SG) prepared by sol-gel calcined at 400°C and 600°C are shown in Fig. 4. These samples show a behavior similar to that observed previously, showing sharp peaks at higher calcination temperatures. This can also be attributed to sintering of the particles after calcination at 600 °C. Moreover, the introduction of manganese in the commercial titania TiO₂-P25 produces a slight shift of both peaks of anatase and rutile, as shown in Table. 2. Concretely, TiO₂-P25 shows peaks at 25.48 and 27.62, while the same peaks appear at 25.39 and 27.56 for the Mn/TiO₂-P25 (Imp-550 °C) sample. This shift, along with the absence of the XRD manganese oxide peaks, may suggest the formation of a solid solution between the titania and manganese, where manganese cations occupy partially Ti⁴⁺ sites. The partial

replacement of the latter by Mn⁴⁺ cations leads to a deformation of the titania red, since the ionic radius of Mn⁴⁺ ions at octahedral sites are known to be 0.670 Å, while that of Ti⁴⁺ ions is 0.745 Å.

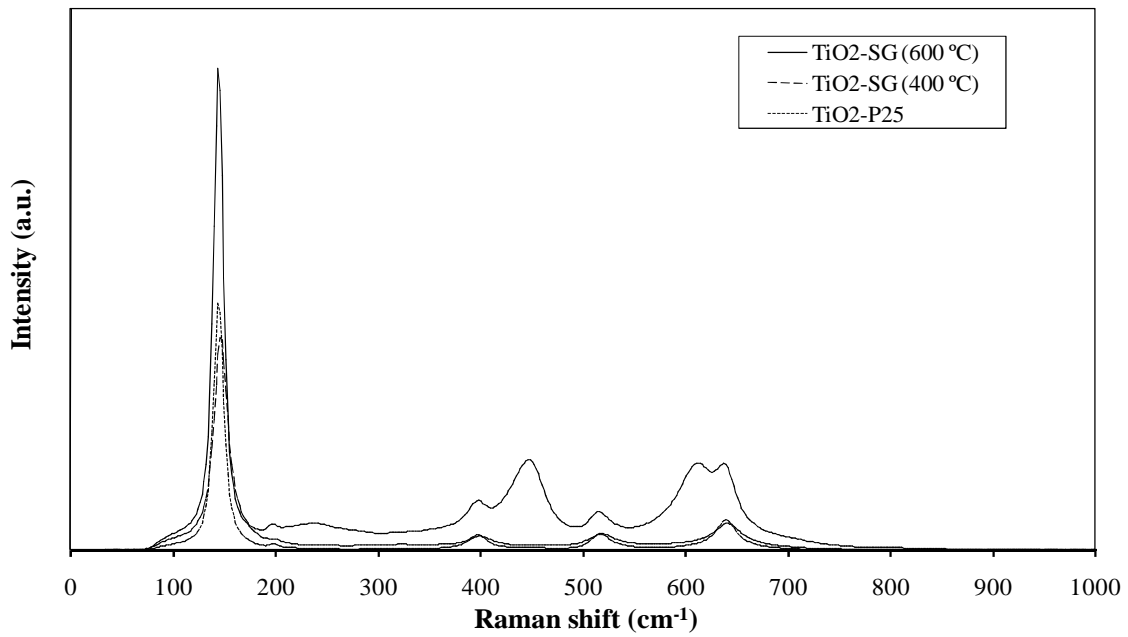


Fig. 6. Raman spectra of the commercial TiO₂-P25 and TiO₂-SG calcined at 400 and 600 °C.

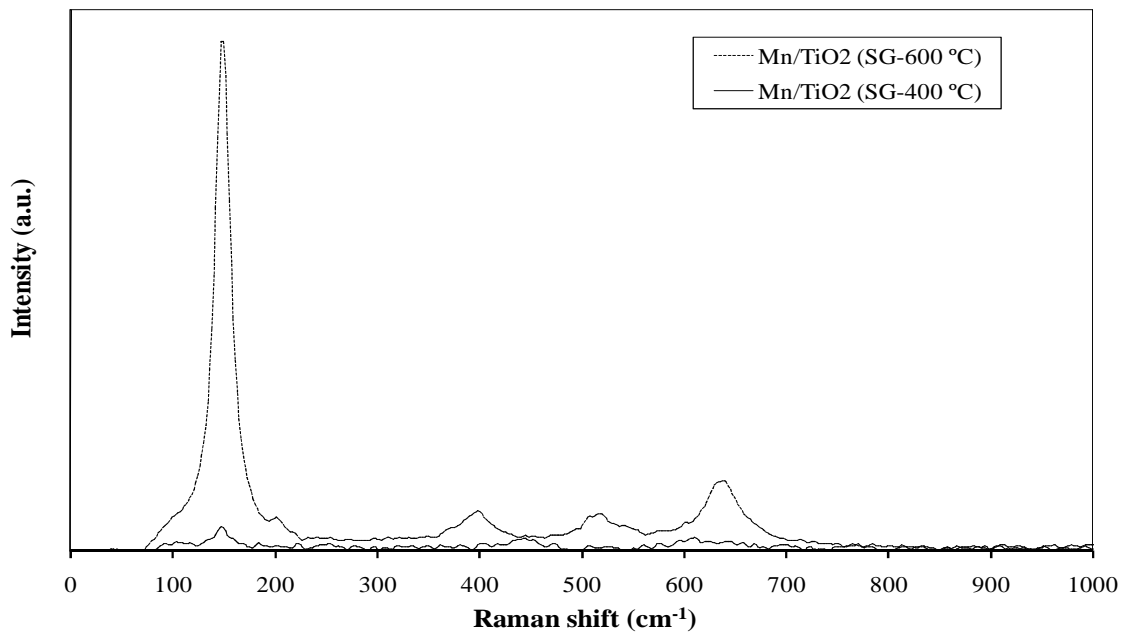


Fig. 7. Raman spectra of Mn/TiO₂ samples prepared by sol-gel and calcined at 400 and 600 °C.

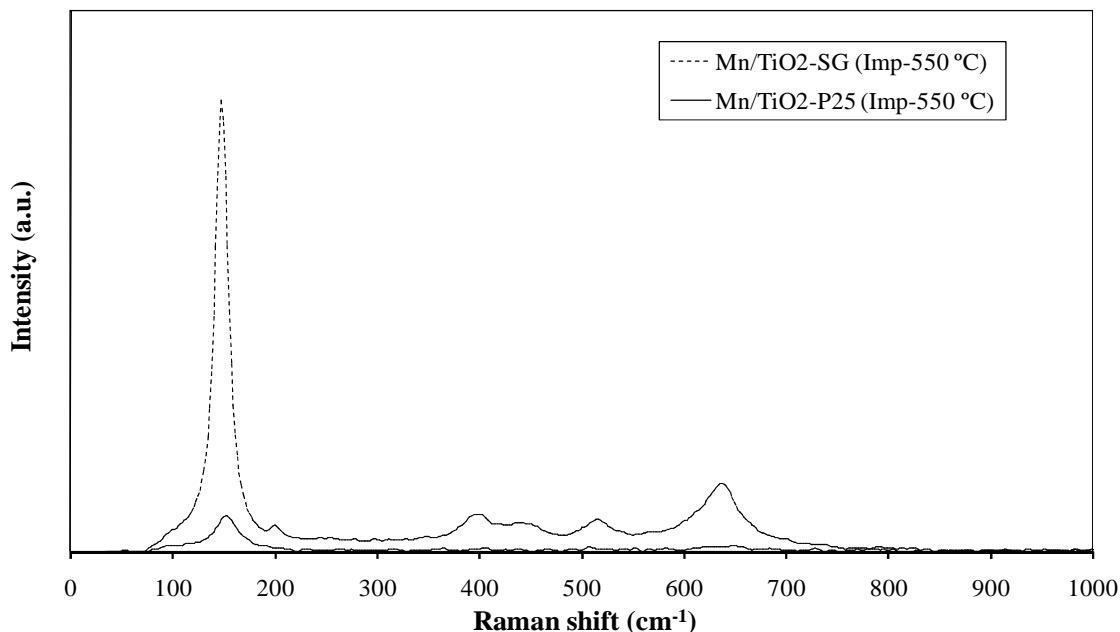


Fig. 8. Raman spectra of Mn/TiO_{2-P25} and Mn/TiO_{2-SG} prepared by impregnation and calcined at 550 °C.

Fig. 6 shows Raman spectra of TiO₂-SG calcined at 400 and 600 °C and the commercial TiO₂-P25 samples. According to the literature, the anatase phase of TiO₂ (D4h¹⁹ (I41 I41/amd)), with a tetragonal structure, presents six active modes of vibration: A_{1g} (519 cm⁻¹), 2B_{1g} (399 and 519 cm⁻¹) and 3E_g (144, 197 and 639 cm⁻¹). The rutile phase (D4h¹⁴ (P42/mnm)), with a similar structure, exhibits four modes of vibration in Raman: A_{1g} (612 cm⁻¹), B_{1g} 143 cm⁻¹, B_{2g} 826 cm⁻¹ and E_g (447 cm⁻¹) [3], [4]. As can be seen, all the samples show five peaks at, approximately, 144, 192, 392, 514 and 631.7 cm⁻¹ characteristic of the anatase phase of TiO₂. However, while TiO₂-SG calcined at 400 °C and TiO₂-P₂₅ samples show only these peaks, the TiO₂ prepared by sol-gel and calcined at 600 °C exhibits other peaks at 444.6 and 607 cm⁻¹, corresponding to the rutile phase. On the other hand, it can be seen that the Raman peaks for TiO₂-SG calcined at 600 °C are more intense than those observed for the other samples. This may be related to the increase of the TiO₂ particle size with the calcination temperature. Several works report that the aspect of TiO₂ Raman bands undergoes different modifications when reducing or increasing the particle size. Thus, the peaks are more or less intense depending on the particles size and even they can be shifted [5]. Fig. 7 shows Raman spectra of Mn/TiO₂(SG) samples prepared by sol-gel method and calcined at 400 and 600 °C. Mn/TiO₂(SG-600 °C) present peaks at 145.6, 195.8, 392.5, 512.1 and 631.6 cm⁻¹, which can be attributed to anatase phase. The same sample calcined at 400 °C shows one broad peak at 145.6 cm⁻¹ with a very low intensity, which could be assigned to anatase phase. The Raman spectrum shape of Mn/TiO₂(SG-400 °C) indicate a material of poor crystallinity or amorphous, which can be due to the low calcination temperature. On the other hand, a slight peaks shift in Mn/TiO₂(SG-600 °C) sample with respect to Manganese-free TiO₂(SG) calcined at the same temperature (Fig. 6) can be observed. This behavior can be explained by the presence of eventual interaction between Mn and TiO₂ [6], [4]. Raman spectra of Mn/TiO_{2-P25} and Mn/TiO_{2-SG} prepared by impregnation and calcined at 550 °C are shown in Fig. 8. Mn/TiO_{2-SG}(Imp-550 °C) exhibits peaks of both anatase and rutile phases at 145.6, 195.8, 392.5, 442.6, 508.2 and 631.6 cm⁻¹. Nevertheless, Mn/TiO_{2-P25} prepared by impregnation and calcined at the same temperature shows a single peak with low intensity at 149.5 cm⁻¹. This may be related to the TiO₂ particles size according to the N₂ adsorption data, which indicate that the BET surface area of Mn/TiO_{2-SG}(Imp-550 °C) is very low compared with Mn/TiO_{2-P25}(Imp-550 °C) and thus the particle are larger. Manganese peaks have not been observed in any case, which may indicate that the particles are highly dispersed with a small particles size on the surface of TiO₂ or they are incorporated into the titania lattice, as indicate the results of N₂ adsorption at -196 °C and XRD.

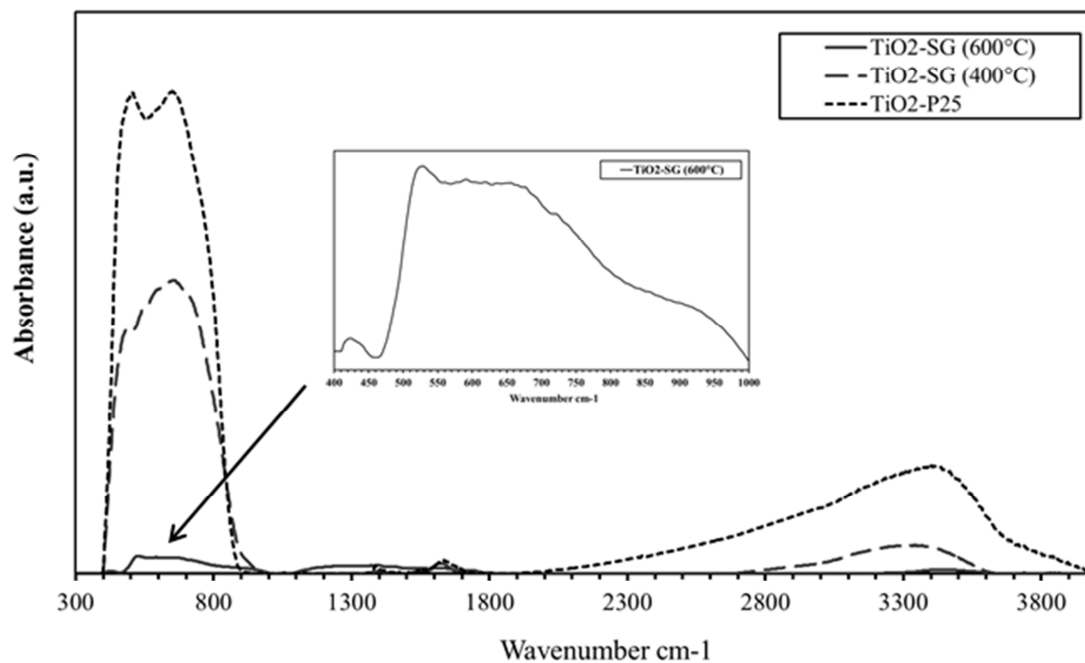


Fig. 9. IR spectra for TiO₂-SG (400 °C), TiO₂-SG (600 °C) and TiO₂-P25 samples.

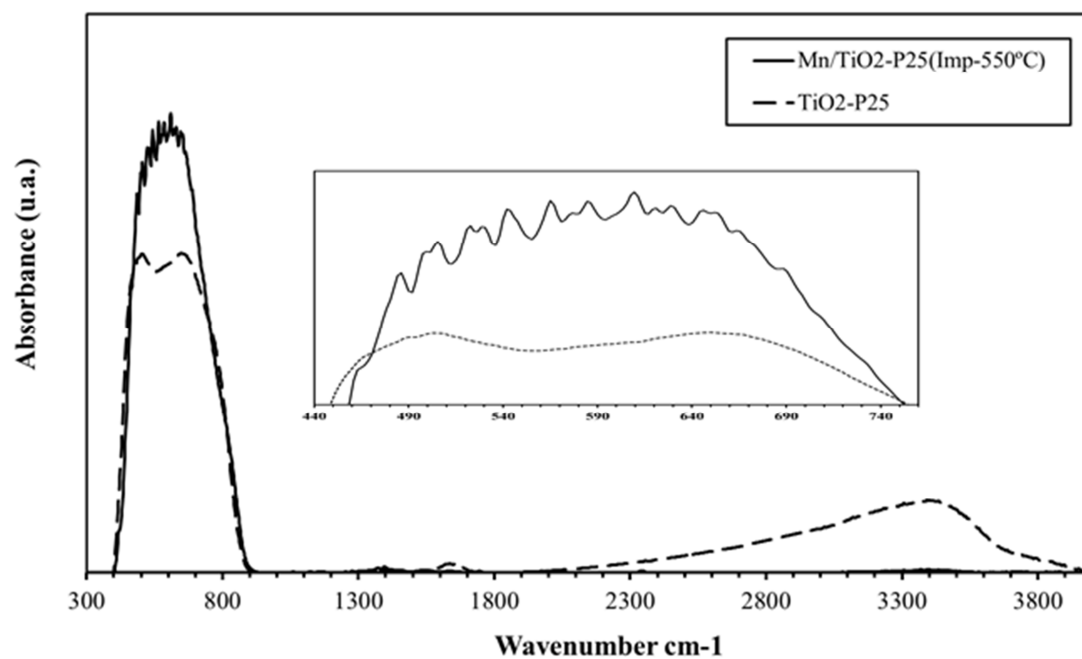


Fig. 10. IR spectra for TiO₂-P25 and Mn/TiO₂ (Imp-550 °C) samples.

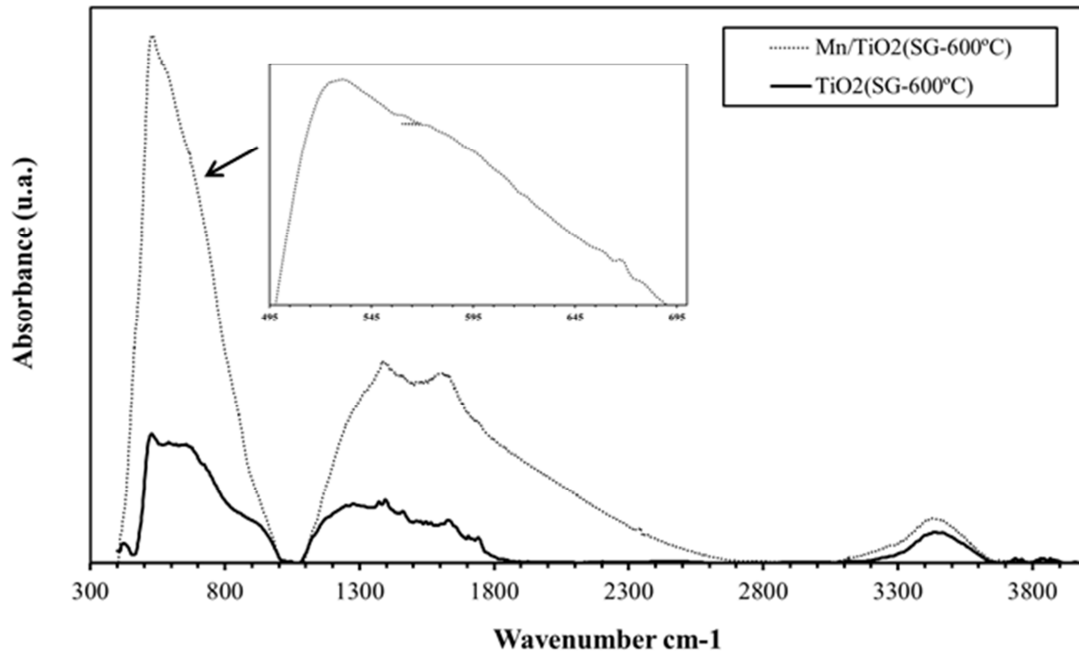


Fig. 11. IR spectra of $\text{TiO}_2(\text{SG-600 } ^\circ\text{C})$ and $\text{Mn/TiO}_2(\text{SG-600 } ^\circ\text{C})$ samples.

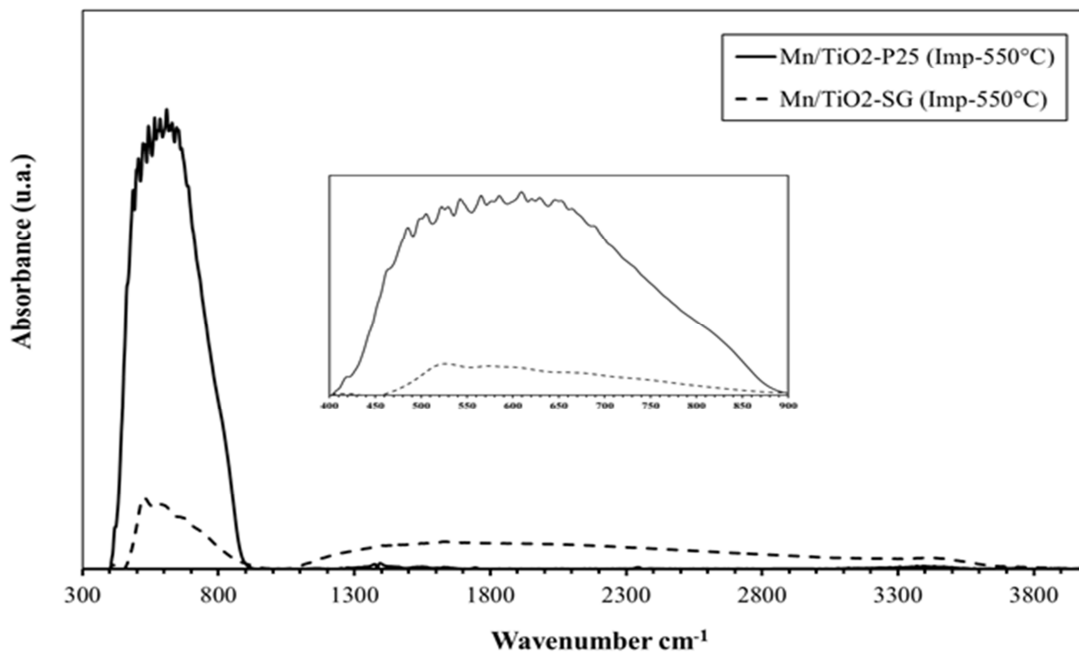


Fig. 12. IR spectra of $\text{Mn/TiO}_2\text{-P25}$ and $\text{Mn/TiO}_2\text{-SG}$ prepared by impregnation and calcined at $550\text{ } ^\circ\text{C}$.

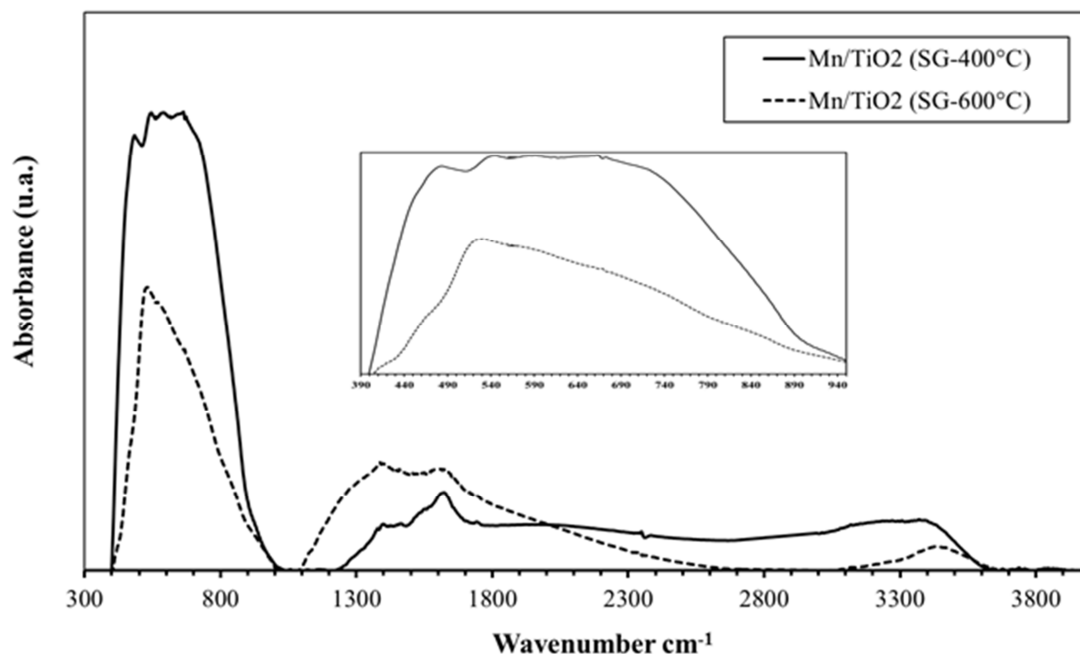


Fig. 13. IR spectra of Mn/TiO₂ prepared by sol-gel and calcined at 400 and 600 °C.

Fig. 9 illustrates FTIR spectra for TiO₂-SG calcined at 400 and 600 °C and the commercial TiO₂-P25 samples. All the samples show absorption band situated at low frequency in the region 400-1000 cm⁻¹ together with a broad band at 1800-4000 cm⁻¹, which can be attributed to hydroxyls groups and adsorbed water. Concretely, TiO₂-SG(400 °C) and TiO₂-P25 show a similar spectra, with a absorption bands centered at 488 and 503 cm⁻¹, which are due to the vibration of Ti-O bond on the TiO₂ lattice. Moreover, the peak appeared at 659.6 cm⁻¹ may be attributed to the vibration of the Ti-O-O bond. TiO₂-SG(600 °C) sample presents in addition to the bands corresponding to O-Ti-O bonds vibration (at 532.3 and 595 cm⁻¹), a peak at 667 cm⁻¹ characteristic of Ti-O vibrational modes of crystalline rutile. Also, a shoulder is observed at 830-1000 cm⁻¹, which may be assigned to stretching vibration of O-O for peroxy groups of the Ti-O-O bonds. Fig. 10 shows IR spectra of TiO₂-P25 and Mn/TiO₂-P25 (Imp-550 °C) samples. The spectrum of the latter shows new peaks, respect to TiO₂-P25 sample, at 655.7 and 690.5 cm⁻¹, which may be related to the vibration modes of β-MnO₂. Also, this sample shows new peaks at 460.9 and 667.4 cm⁻¹ characteristics of rutile mode vibration of Ti-O bonds. The spectrum of the sample Mn/TiO₂(SG-600 °C) illustrated in Fig. 11 shows a band at 667.3 cm⁻¹ which can be assigned to Ti-O vibrational modes of rutile. Moreover, two peaks appear at 533 and 620 cm⁻¹ which correspond to Mn-O-Ti and O-Ti-O vibrational modes. Fig. 12 shows FTIR spectra of Mn/TiO₂-P25 y Mn/TiO₂-SG samples prepared by impregnation and calcined at 550 °C. Mn/TiO₂-SG (Imp-550 °C) shows no peak associated with vibrational modes of rutile. However, the bands appearing at 659.6 and 671.2 cm⁻¹ can be attributed to the formation of β-MnO₂ and α-Mn₂O₃ phases. The spectrum of Mn/TiO₂-SG (400 °C) prepared by sol-gel and calcined at 400 °C (Fig. 13) shows one peaks at 663.5 cm⁻¹ which can be assigned to Ti-O vibrational modes of rutile. On the other hand, the bands located at 484.1 and 613.3 cm⁻¹ may indicate the presence of α-Mn₂O₃ phase, although the identification of MnO_x species in these catalysts is rather difficult since their bands overlap with those of the support. Furthermore, MnO₂ and Mn₂O₃ phases of manganese oxide exhibit very close IR bands and therefore the assignment of these bands is very difficult [7], [8], [9], [10].

3.2 PHOTODEGRADATION OF PHENOL

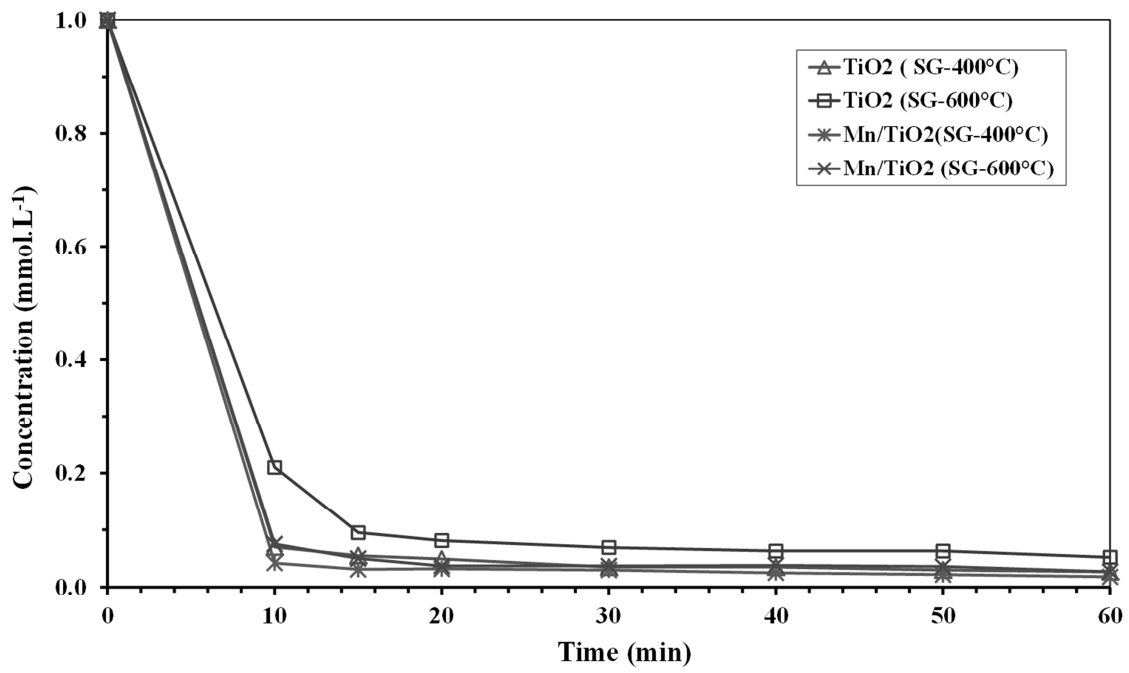


Fig. 11. Kinetic behavior of phenol degradation by TiO₂ and Mn/TiO₂ photocatalysts prepared by sol-gel and calcined at 400 and 600 °C

As has been mentioned above, the photocatalytic activity of the prepared catalysts has been evaluated in phenol degradation in aqueous solution. Fig. 11 plots kinetic behavior of phenol degradation for TiO₂ and Mn/TiO₂ prepared by sol-gel and calcined at 400 and 600 °C. TiO₂ calcined at 400 °C exhibits higher activity than the same sample calcined at 600 °C. This could be due to the high surface area of the TiO₂-SG (400 °C) with respect to TiO₂-SG (600 °C). On the other hand, the introduction of manganese improves the photocatalytic behavior of titania in the photodegradation of phenol, as expected, independently of the calcination temperature used. Thus, TiO₂-SG (400 °C) achieves a removal rate of 94.8% while phenol conversion exhibited by Mn/TiO₂, prepared in the same conditions, is approximately 98.2%.

On the other hand, the degradation starts with a fast kinetic at short contact time (10 min) and slows down to become practically constant. This behavior can be related to the deactivation of the catalysts. Several studies related to the oxidation of phenols have reported this behavior and attributed it to the deactivation of the catalyst active site by the by-products of the phenol oxidation. Thus, during the reaction of phenol oxidation, the latter decomposes giving rise to several by-products which adsorb strongly (chemisorption) on the surface of the catalyst, leading to catalyst deactivation [11].

4 CONCLUSIONS

This main aim of the present study was, firstly, the preparation of catalysts with dioxide of titanium TiO₂, and then their application in the photodegradation of the phenol from aqueous solutions. The TiO₂ catalysts were prepared by two different methods: sol-gel and incipient witness impregnation methods, and then modified by manganese introduction, in order to improve its photocatalytic activity.

N₂ adsorption at -196 °C data showed that the BET surface area decrease considerably with increasing the calcination temperature due to the increase of the particle size during the calcination. The introduction of manganese produces a decrease of the BET surface of Mn/TiO₂ prepared by sol-gel, due to a partial blockage of the porosity by manganese particles. However, the introduction of manganese on the commercial titania (P25) result in a augmentation of BET surface area, which can be indicate the introduction of manganese into the interstitial sites of TiO₂ lattice leading to a decrease in the crystallite size. The Thermal analysis, Raman, XRD and IR data confirmed the presence of both phases of TiO₂ (Anatase and rutile) in some samples, depending on the calcination temperature. IR results revealed the presence of different manganese oxide phases in the prepared catalysts.

The prepared catalysts were employed in the photodegradation of phenol. The obtained results indicate a practically complete degradation (98.2% for Mn/TiO₂ (SG- 400 °C)), reached after 10 min of reaction.

REFERENCES

- [1] V. Brezová, A. Blazková, L. Karpinsky, J. Groskova, B. Havlinová, V. Jorik and M. Ceppan, , "Phenol decomposition using Mⁿ⁺/TiO₂ photocatalysts supported by the sol-gel technique on glass fibres," *Journal of photochemistry and photobiology. A: Chemistry*, vol. 109, no.2, pp. 177 – 183, 1997.
- [2] A.E. Shalan and M.M. Rashad, "Incorporation of Mn²⁺ and Co²⁺ to TiO₂ nanoparticles and the performance of dye-sensitized solar cells," *Applied Surface Science*, vol. 283, pp. 975 – 981, 2013.
- [3] W.G. Fateiey, N.T. McDevitt and F.F. Bentley, "Infrared and Raman Selection Rules for Lattice Vibrations: The Correlation Method," *Applied Spectroscopy*, vol. 25, no. 2, pp. 155 – 173, 1971.
- [4] J.P. Xu, S.B. Shi, L. Li, J.F. Wang, , L.Y. Lv, F.M. Zhang, and Y.W. Du, "Effect of manganese ions concentration on the anatase-rutile phase transformation of TiO₂ films," *Journal of Physics and Chemistry of Solids*, vol. 70, no. 3 - 4, pp. 511 – 515, 2009.
- [5] H.C. Choi, Y.M. Jung and S.B. Kim, "Size effects in the Raman spectra of TiO₂ nanoparticles," *Vibrational Spectroscopy*, vol. 37, no. 1, pp. 33 – 38, 2005.
- [6] F.M. Liu, T.M. Wang, J.Q. Li, C. Wang, S.K. Zheng and M. Duan, "Structural, Optical and magnetic properties of a Mn thin film sandwiched between TiO₂ films prepared by magnetron sputtering," *Journal of Magnetism and Magnetic Materials* , vol. 251, no. 3, pp. 245 – 250, 2002.
- [7] F. Buciuman, F. Patcas, R. Craciun and D.R.T. Zahn, "Vibrational spectroscopy of bulk and supported manganese oxides," *Physical Chemistry Chemical Physics*, vol. 1, no. 1, pp. 185 – 190, 1999.
- [8] L. Kernazhitsky, V. Shymanovska, T. Gavrilko, G. Puchkovska, V. Naumov, T. Khalyavka, V. Kshnyakin, V. Chernyak and J. Baran, "Titanium-Manganese oxides. Optical and photocatalytic properties," *Journal of Nano- and Electronic Physics*, vol. 2 no. 2, pp. 83 – 95, 2010.
- [9] I. Othman, R.M. Mohamed, and F.M. Ibrahim, "Study of photocatalytic oxidation of indigo carmine dye on Mn-supported TiO₂," *Journal of Photochemistry and Photobiology. A: Chemistry*, vol. 189, no. 1, pp. 80 – 85, 2007.
- [10] A. Šurca Vuk, R. Jese, M. Gaberscek, B. Orel and G. Drazic, "Structural and spectroelectrochemical (UV-vis and IR) studies of nanocrystalline sol-gel derived TiO₂ films," *Solar Energy Materials & Solar Cells*, vol. 90, no. 4, pp. 452 – 468, 2006.
- [11] S. Nouisir, , S.Keav, , Jr.b. Barbier, M. Bensitel, R. Brahmi, D. Duprez, "Deactivation phenomena during catalytic wet air oxidation (CWAO) of phenol over platinum catalysts supported on ceria and ceria-zirconia mixed oxides," *Applied Catalysis. B: Environmental*, vol. 84, no. 3-4, pp. 723 – 731, 2008.